An Intelligent Tool for Anatomical Object Segmentation Using Deformable Surfaces

Konstantinos K. Delibasis, Argiris Christodoulidis, and Ilias Maglogiannis

Dept. of Computer Science & Biomedical Informatics, University of Central Greece, Lamia, Greece, Lamia
kdelibasis@yahoo.com,
{axristodoulidhs,imaglo}@ucg.gr

Abstract. Image segmentation is a very active area of research in machine vision. In this work, an innovative methodology is presented that allows the segmentation of objects in three-dimensional images with initial user intervention. The paper describes the adopted approach for implementing the algorithm of deformable / active surfaces (AS), using the explicit scheme for numerical evaluation of the partial derivative equation of the AS evolution. Both the Vector Field Convolution (VFC) and the Gradient Vector Flow (GVF) image dynamic field are investigated for 3D segmentation using the AS. The proposed methodology is implemented as software tool, which allows the initialization of AS using cylinder-like surfaces with user intervention. Initial results are provided for the case of three-dimensional synthetic data and clinical Computed Tomography (CT) images, in terms of segmentation accuracy and speed of convergence.

Keywords: Computer Vision, Deformable surface, Active surfaces, Object segmentation.

1 Introduction

Image segmentation is a central problem in computer vision. Object segmentation from three-dimensional images is a special, more demanding case of this task, which finds numerous applications in automated diagnosis, medical decision support systems and medical treatment planning and assessment. The concept of active contours for image segmentation was first reported for segmenting objects of interest in [1]. Since then, the methodology of active contours and active surfaces has been widely reported in literature [2]. A number of variants have been applied, using several image-based definitions of the external force field. In [3] an internal force component parallel to the contour outward normal vector was introduced to simulate the inflating balloon effect. The image edge strength is utilized in [1], the Gradient Vector flow (GVF) [4], [5] and the Vector Field Convolution (VFC) [6] are more recent advances. Almost all active surface approaches require proper initialization when applied to images with multiple objects. In this work, we propose an explicit scheme for the evolution equation of an Active Surface (AS) model. The AS model is constructed on

I. Maglogiannis, V. Plagianakos, and I. Vlahavas (Eds.): SETN 2012, LNAI 7297, pp. 206–213, 2012.

a rectangular grid rather on a Delaunay triangular mesh, allowing simpler arithmetic operations for calculating partial derivatives. A software tool is developed for providing the AS model with user-based initialization using simple cylinder-like surfaces. The rest of the paper is structured as follows: Section 2 presents the proposed methodology for AS evolution, while Section 3 reports the results obtained by the evaluation of the method. Finally, Section 4 concludes the paper.

2 Methodology

2.1 Active Surface (AS) Explicit Evolution

In this section we present the adopted mathematical modelling approach for the AS evolution. Let us define the deformable contour (snake) consisting of N_p points at time t, as $\mathbf{v}(s,t) = \mathbf{v}_t(s) = \left(x_t(s), y_t(s), z_t(s)\right)^T$, with $s \in \left[1, N_p\right]$. According to [8] the evolution of an active contour $\mathbf{v}(s,t)$, under the influence of external force field $\mathbf{f}_{ext}\left(\mathbf{v}(s,t)\right)$ is given by

$$\frac{\partial \mathbf{v}(s,t)}{\partial t} = a\mathbf{v}''(s,t) - \beta\mathbf{v}''''(s,t) + \mathbf{f}_{ext}\left(\mathbf{v}(s,t)\right) \tag{1}$$

where the $\mathbf{v}''(s,t), \mathbf{v}''''(s,t)$ are the 2nd and 4th derivative order with respect to parameter contour parameter s and a, β are parameters controlling the shape of the snake.

In the case of the active (or deformable) surface $\mathbf{v}(s,u,t)$ at time t, consisting of N_c contours with N_p points each, as $\mathbf{v}(s,u,t) = \left(x_t(s,u), y_t(s,u), z_t(s,u)\right)^T$, with $(s,u) \in \left[1, N_c\right] \times \left[1, N_p\right]$ the AS evolution equation is similar to (1):

$$\frac{\partial \mathbf{v}(s,u,t)}{\partial t} = a\mathbf{v}''(s,u,t) - \beta\mathbf{v}''''(s,u,t) + \mathbf{f}_{ext}\left(\mathbf{v}(s,u,t)\right) \tag{2}$$

Eq. (2) can generate 3 partial differential equations (PDE), one for each Cartesian coordinates of the AS points. The 2nd and forth order derivative in (2) are calculated as following:

$$\begin{aligned} \mathbf{v}'' &= \frac{\partial^2 \mathbf{v}}{\partial s^2} + \frac{\partial^2 \mathbf{v}}{\partial u^2} = \mathbf{v}_{ss} + \mathbf{v}_{uu}, \\ \mathbf{v}'''' &= \frac{\partial^4 \mathbf{v}}{\partial s^4} + \frac{\partial^4 \mathbf{v}}{\partial u^4} = \mathbf{v}_{ssss} + \mathbf{v}_{uuuu} \end{aligned} \tag{3}$$

The above partial derivatives can be arithmetically approximated using central differences, independently along the s (contours) and u parameters. If we temporarily drop the time parameter symbol t, the partial derivatives of the active surface along the s parameter are approximated as following:

$$\begin{aligned}
&\mathbf{v}_{ss}(s,u) = [1,-2,1] * \mathbf{v}(s,u) = \mathbf{v}(s+1,u) - 2\mathbf{v}(s,u) + \mathbf{v}(s-1,u) \\
&\mathbf{v}_{ssss}(s,u) = [1,-4,6,-4,1] * \mathbf{v}(s,u) \\
&= \mathbf{v}(s+2,u) - 4\mathbf{v}(s+1,u) + 6\mathbf{v}(s,u) - 4\mathbf{v}(s-1,u) + \mathbf{v}(s-2,u)
\end{aligned} \tag{4}$$

where the * stands for the linear convolution operator. We can enforce closed contours along the s or u parameter by using modulo operations for the point parameters [7, p.9] i.e. $\mathbf{v}_{ss}(1,u) = [1,-2,1] * \mathbf{v}(s,u) = \mathbf{v}(s+1,u) - 2\mathbf{v}(s,u) + \mathbf{v}(N_p,u)$.

By discretising the time derivative in (2), we obtain the discrete AS evolution equation, in a manner similar to [5, (A10)]:

$$\begin{aligned}
&\frac{\mathbf{v}^{t+\Delta t}(s,u) - \mathbf{v}^{t}(s,u)}{\Delta t} = a\mathbf{v}^{t}_{ss} + a\mathbf{v}^{t}_{uu} - \beta\mathbf{v}^{t}_{ssss} - \beta\mathbf{v}^{t}_{uuuu} + \mathbf{f}_{ext}\left(\mathbf{v}^{t}(s,u)\right) \\
&\mathbf{v}^{t+\Delta t}(s,u) = \mathbf{v}^{t}(s,u) + \Delta t\left(a\mathbf{v}^{t}_{ss} + a\mathbf{v}^{t}_{uu} - \beta\mathbf{v}^{t}_{ssss} - \beta\mathbf{v}^{t}_{uuuu} + \mathbf{f}_{ext}\left(\mathbf{v}^{t}(s,u)\right)\right)
\end{aligned} \tag{5}$$

The above equation is the forward Euler arithmetic approximation of the active surface PDE, often called explicit PDE scheme [11]. We utilized this approach, since the implicit PDE approximation, as described in [6, Eq.(9)], [7] would require the inversion of an NxN pentadiagonal matrix, with N=N_cxN_p, for each time iteration. Despite the fact that efficient techniques exist for inverting such tables [9], [10], the size of the matrix imposes prohibitive memory requirements (N may easily be of the order of 10^4 – see Table 1). Eq. (5) converges without numerical instability for $\Delta t < 0.25$ [8]. The parameters a in (2), (5) was set to 0.2 for anatomical objects and 0.25 for synthetic data, whereas and the parameter β was set to 0.1 for anatomical objects and 0.2 for synthetic data, as determined experimentally.

The AS is allowed to iterate until the average positional difference between two consecutive iterations falls below the threshold of 0.1 pixels.

2.2 Definition of External Force Field

In order to calculate the corresponding AS model external forces, we utilize the Vector Field Convolution (VFC) [6], which was reported to be superior to the Gradient Vector Flow image dynamic field, described in [4]. VFC is generated using a kernel **K** containing vectors that point towards the origin of K. The magnitude of the vectors is calculated using [6 (15)] setting the γ parameter to 2.2. The size of the kernel **K** was set to 32 pixels for both trachea/synthetic data in [6 (17)]). The GVF force field is generated using a homogeneous diffusion of the original image gradient vector. Each iteration of the diffusion operation is performed using 2D convolution with the

following matrix $\begin{bmatrix} 0 & \mu & 0 \\ \mu & 1-4\mu & \mu \\ 0 & \mu & 0 \end{bmatrix}$ as described in [7, Eq.(26)], with μ=0.2. The number of iterations for implementing the diffusion of the image gradient was set to 100. For the implementation of the VFC and GVF, the Matlab source code, which is available in [6] was used.

2.3 User Intervention

The user may intervene in a number of ways in order to optimise the segmentation results. The most important intervention is the initialization of the Active Surface, since it directly affects the correct convergence and the segmentation accuracy of the AS model. The main objective is the use of simple initializing shapes, easy to be defined by the used, whereas achieving sufficient proximity to the required object. In this work we utilize two kinds of cylinder-like initializing surfaces: a) a homogenous cylinder with a straight vertical axis and b) a non-homogeneous cylinder (variable radius) with C^0 continuous axis. We choose this type of initialization because of its simplicity and ease of user-based input.

3 Results

Results are presented using both 3D synthetic data and anatomical objects from CT images. We used the two-dimensional (2D) synthetic data of [4], [6] to create a 64x64x64 raw volume as shown in Fig.1. This shape has been used extensively for Active Contour / AS testing, since it is characterized by a deep and narrow cut that cannot easily be discovered by the AC/AS methods.

The AS is initialized using variable radius straight axis cylinder (Fig. 1b), consisting of 64 contours with 320 points each. The final AS using the VFC external force field is shown in Fig. 1c, after 260 iterations, with execution time equal to 99 sec using Matlab 7.9.0, running on a laptop with i5 at 2.40 GHz CPU and 4GB of RAM. It is evident that the AS has converged to the correct shape, despite the difficulty presented by the required shape. The intersection of the converged AS with the mid-slice of the synthetic volume data (Fig. d) confirms visually the accuracy of the segmentation. The average distance of the AS points from the shape edge voxels was 0.195 voxels.

In Fig.2 a comparison of the total positional error (in voxels) of the converged AS under the GVF and the VFC external force field is shown for the synthetic volume data. It can be observed that the VFC converges faster and more accurately than the GVF. The intersection of the AS with slice 32 is given for selected iterations (the last iteration for both cases is included).

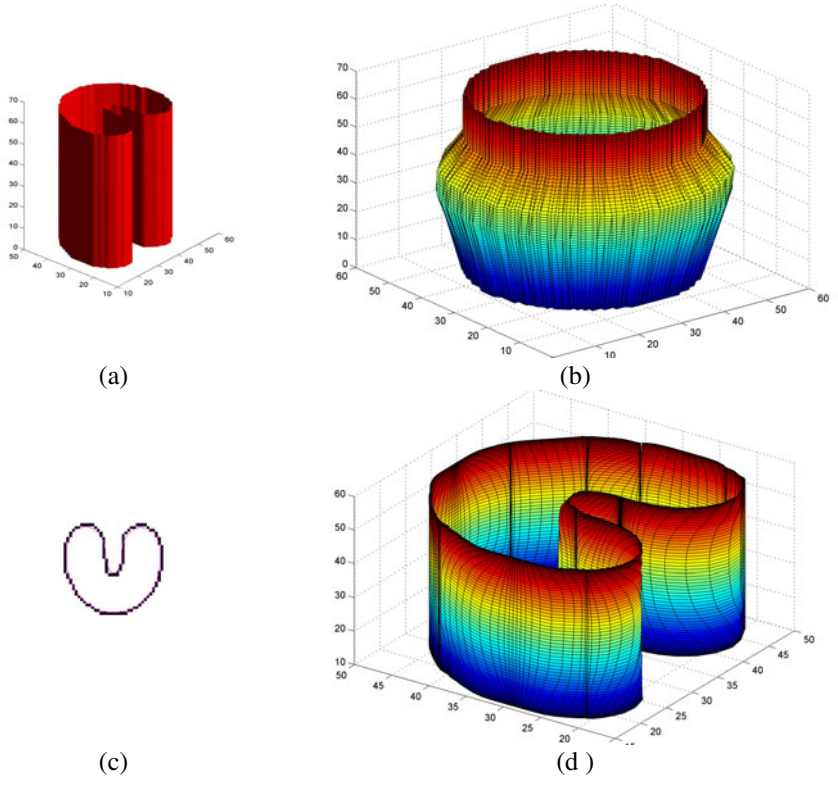

Fig. 1. Segmentation of 3D synthetic data (a) using AS initialized as a cylinder-like surface (b). The converged AS and its intersection with the mid-slice of the 3D data is shown in (d) and (c).

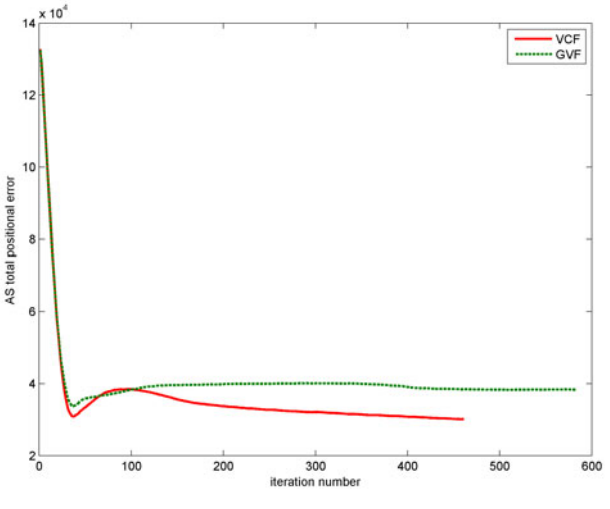

Fig. 2. The evolution of the AS positional error in the case of 3D synthetic data, using VFC and GVF external force field

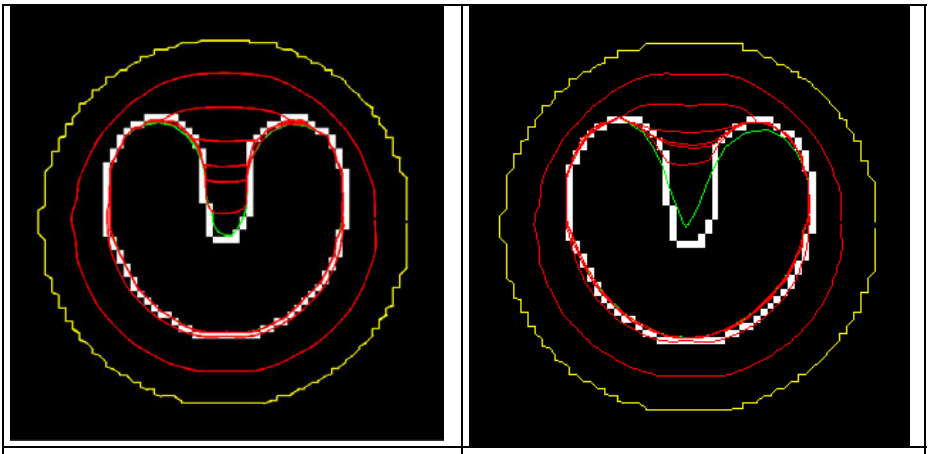

(a) (b)

Fig. 3. (a) The evolution of AS under VFC (iterations 1,20,40,60,80,100,200,460) and (b) GVF (iterations 1,20,40,60,80,100,200,581)

In Fig.4 the results of segmenting a part of the trachea are presented using AS with GVF and VFC. The AS is initialized by the used as the cylinder in Fig.3a. User initialization was performed in 5 out of the 40 processed transverse slices, inside the required object. The converged AS using GVF and VFC is shown in (b) and (c) respectively). The intersection of the initial AS model, the AS at the 10th iteration and the converged AS is also given for VFC and GVF in (d) and (e) respectively. It can be observed that the segmentation performed by the VFC appears more accurate than the AS under the GVF external forces.

The numerical results from the performed experiments are presented in Table 1. The average positional error in the case of the anatomical objects was calculated based on object delineation by expert user. It becomes obvious that the proposed tool can find practical use in a research and even in a clinical environment, since it allows object segmentation from 3D data with low degree of user intervention. The VFC appears to converge slightly faster and more accurately both in synthetic data and clinical volumes.

Table 1. Numeric results form the AS-based object segmentation

Object	Method	N_cxN_p	Num. of iterations	Average positional error (voxels)
Synthetic	GVF	64x320	581	0.149
	VFC	64x320	460	0.097
Trachea I	GFV	42x70	155	0.81
	VFC	42x70	148	0.72
Trachea II	GVF	40x80	112	1.02
	VFC	40x80	91	1.12

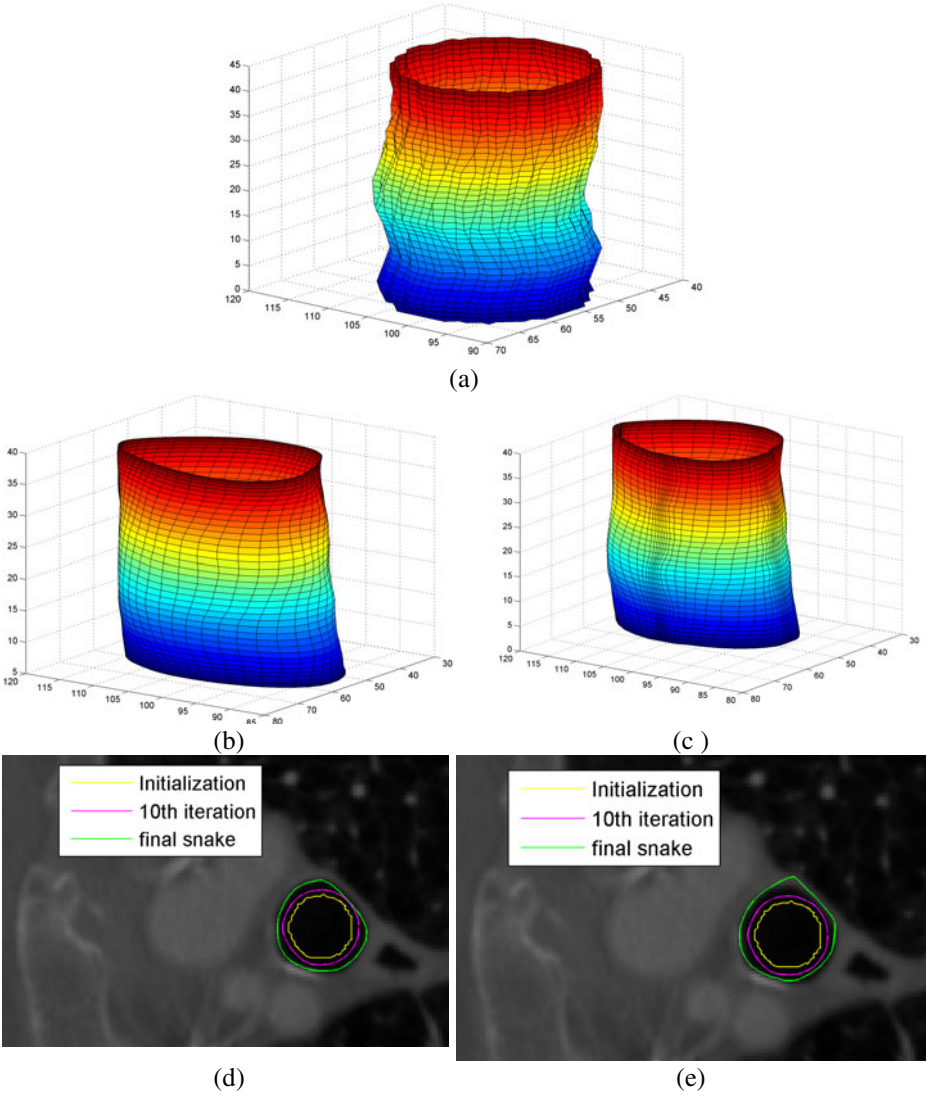

Fig. 4. Segmentation of the trachea with AS initialized in (a), using VFC (b) and GVF (c). The intersection of the initial AS, the AS at the 10th iteration and the converged AS is also given for VFC and GVF in (d) and (e) respectively.

4 Conclusions

In this paper we presented a novel 3D segmentation methodology based on AS modelling, which has been implemented as an intelligent software tool. The developed tool has been tested in both synthetic and clinical data. In both cases the accuracy of the evolved model is quite satisfactory. The corresponding quantitative and qualitative results from the visual assessment show that the proposed method is capable of accurately modeling anatomical structures, requiring only limited user intervention.

References

1. Kass, M., Witkin, A., Terzopoulos, D.: Snakes: Active contour models. International Journal of Computer Vision 1(4), 321–331 (1988)
2. He, L., Peng, Z., Everding, B., Wang, X., Han, C.Y., Weiss, K.L., Wee, W.G.: A comparative study of deformable contour methods, on medical image segmentation. Image and Vision Computing 26, 141–163 (2008)
3. Cohen, L.D.: On active contour models and balloons. Computer Vision, Graphics, and Image Processing. Image Understanding 53(2), 211–218 (1991)
4. Xu, C., Prince, J.L.: Snakes, shapes, and gradient vector. IEEE Transactions on Image Processing 7(3), 359–369 (1998)
5. Xu, C.: Deformable Models with application to human cerebral cortex reconstruction from Magnetic Resonance images, PhD dissertation Johns Hopkins University (1999)
6. Li, B., Acton, S.T.: Active contour external force using vector field convolution for image segmentation. IEEE Transactions on Image Processing 16, 2096–2106 (2007)
7. Acton, S., Ray, N.: Biomedical Image Analysis: Segmentation. Morgan and Claypool Publishers (2009) ISBN: 9781598290219
8. Heat, M.T.: Scientific Computing, An Introductory Survey, 2nd edn. McGraw-Hill (2002) ISBN 007112229X
9. Press, W., Teukolsky, S., Vetterling, W., Flannery, B.: Numerical Recipes in C, 2nd edn. Cambridge Univ. Press, Cambridge (1992)
10. Benson, A., Evans, D.J.: A normalized algorithm for solution of positive definite symmetric quindiagonal systems of linear equations. ACM Trans. Math. Softw. 3, 96–103 (1977)
11. Hall, C.A., Porsching, T.A.: Numerical analysis of partial differential equations. Englewood Cliffs, Prentice Hall (1990)